Mechanistic Insights on the Functionalization of CO_2 with Amines and Hydrosilanes Catalyzed by a Zwitterionic Iridium Carboxylate-Functionalized Bis-NHC Catalyst

Ana I. Ojeda-Amador,[a] Julen Munarriz,[b] Pablo Alamán-Valtierra,[a] Víctor Polo,[b] Raquel Puerta-Oteo,[a] M. Victoria Jiménez,[a] Francisco J. Fernández-Alvarez*,[a] and Jesús J. Pérez-Torrente*,[a]

Dedication

Abstract: The zwitterionic complex [Cp*IrCl{(MeIm)$_2$CHCOO}] (**1**) efficiently catalyzes the selective hydrosilylation of CO_2 to afford the corresponding silylformate. The best reaction performance has been achieved in acetonitrile at 348 K using $HSiMe_2Ph$. The **1**-catalyzed reaction of pyrrolidine with CO_2 and $HSiMe_2Ph$ strongly depends on the CO_2 pressure. At low concentration of CO_2 (1 bar) formation of the corresponding silycarbamate, by insertion of CO_2 into the Si–N bond of the in situ generated silylamine was observed, while at higher pressure (3 bar) the formamide derivative was obtained as major reaction product. The unexpected formation of pyrrolidin-1-ium formate as intermediate of the reaction the **1**-catalyzed of CO_2 with pyrrolidine and $HSiMe_2Ph$ has been observed, and its role in the formation of 1-formylpyrrolidine rationalized. Moreover, a mechanism for the reaction of CO_2 with hydrosilanes, in the presence and in the absence of amines, based on theoretical calculations has been proposed.

Introduction

Nowadays, there is an increasing interest in developing chemical processes that allow using carbon dioxide as a C1 carbon source for the industrial preparation of value-added chemicals.[1] The reasons, beyond the well-known problem of the increase in the concentration of CO_2 in the Earth atmosphere, are related to its low toxicity, abundance and availability.[1a,1b]

The catalytic reaction of CO_2 with hydrosilanes has emerged as a thermodynamically favored procedure that allows for the reduction of CO_2 under mild reaction conditions.[2] Nonetheless, this methodology faces lack of selectivity, as silylformates are usually obtained among other products, such as bis(silyl)acetals, methoxysilanes and methane, in variable relative amounts (Scheme 1).[3] In this sense, it should be noted that during the last few years, several examples of effective catalytic systems for the selective reduction of CO_2 with hydrosilanes to give silylformates[4-10] bis(silyl)acetals,[11] methoxysilanes[12] or methane[13] have been reported. Moreover, some catalysts have also been employed for the formylation and/or subsequent methylation of N–H amine bonds by their reaction with CO_2 and hydrosilanes.[14] This methodology has also been recently employed to prepare unsymmetrical aminals[15] and spiroindolepyrrolidines.[16]

N-heterocyclic carbenes (NHCs) are now ubiquitous in organometallic chemistry and catalysis because of their strong coordination ability and tunable character, which facilitates the control of the steric and electronic properties at the metal center.[17,18] The chelate effect derived from coordination of bis-NHC ligands results in a stable metal-ligand platform with easily modulable properties.[19] In this context, it is worth noting that iridium(III) bis-NHC complexes have been reported as active and selective catalysts for the hydrosilylation of alkynes.[20,21] However, it draws attention that examples of CO_2 hydrosilylation catalysts based on iridium(III) bis-NHC species have not been so far reported.

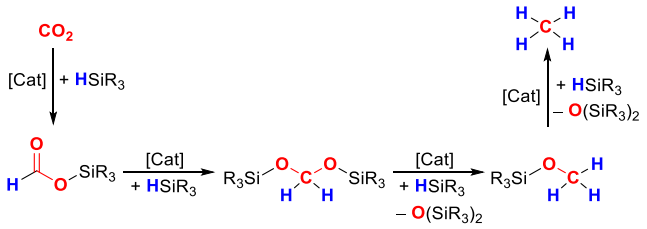

Scheme 1. Stepwise reduction of CO_2 to methane with hydrosilanes.

We have recently focused our attention on the potential of a carboxylate-functionalized methylene-bridged bis-NHC ligand for the construction of a versatile metal-ligand platform with application in catalysis.[22] In this regard, we have shown that the carboxylate group at the linker provides hemilabile properties to the ligand, allowing for the stabilization of catalytic intermediates through the κ^3-*C,C',O*-tridentate coordination mode.[23] However, in most complexes the bis-NHC ligand exhibits a κ^2-*C,C* bidentate coordination mode with an uncoordinated functional group in the skeleton that has shown to be a reactive site.[22]

As a continuation of our studies on the catalytic applications of functionalized bis-NHC metal complexes, we have found that the zwitterionic complex, [Cp*IrCl{(MeIm)$_2$CHCOO}] (**1**) (MeIm = 3-methylimidazol-2-yliden-1-yl),[22] which features a carboxylate bridge-functionalized bis-NHC ligand efficiently catalyzes the reduction of CO_2 with hydrosilanes to selectively afford the

[a] Dr. A. I. Ojeda-Amador, M.Sci. P. Alamán-Valtierra Dr. R. Puerta-Oteo, Prof. Dr. M. V. Jiménez, Prof. Dr. F. J. Fernández-Alvarez, and Prof. Dr. J. J. Pérez-Torrente
Departamento de Química Inorgánica – Instituto de Síntesis Química y Catálisis Homogénea (ISQCH). Universidad de Zaragoza. Facultad de Ciencias 50009, Zaragoza – Spain, e-mail: paco@unizar.es, perez@unizar.es
[b] Dr. J. Munarriz, Prof. Dr. V. Polo
Departamento de Química Física – Instituto de Biocomputación y Física de Sistemas complejos (BIFI) – Universidad de Zaragoza. Facultad de Ciencias 50009, Zaragoza – Spain.

corresponding silylformates. The investigation of the reaction mechanism has disclosed the key role of the uncoordinated carboxylate fragment on the catalytic performance. In addition, the catalytic activity in the reductive functionalization of CO_2 with amines and hydrosilanes, which combines both CO_2 reduction and C–N bond formation, has also been investigated. Moreover, the reaction mechanism for the reduction of CO_2 with hydrosilanes, both in the presence and in the absence of amines, has been studied by theoretical calculations.

Results and Discussion

Catalytic hydrosilylation of carbon dioxide. The zwitterionic iridium(III) derivative **1** has proven to be an active catalyst precursor for the selective reduction of CO_2 with hydrosilanes to afford the corresponding silylformate (Scheme 2).

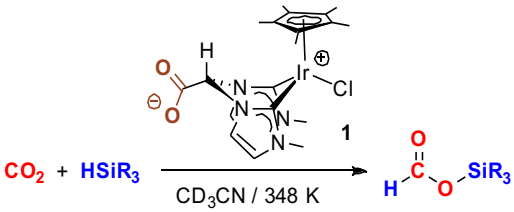

Scheme 2. CO_2 hydrosilylation catalyzed by the zwitterionic iridium(III) compound [Cp*IrCl{(MeIm)$_2$CHCOO}] (**1**) (SiR_3 = $SiEt_3$, **2a**; $SiMe_2Ph$, **2b**; $SiMePh_2$, **2c**; $SiMe(OSiMe_3)_2$, **2d**).

The **1**-catalyzed reaction of CO_2 (3 bar) with $HSiEt_3$ was investigated as a test bench to explore the viability of using **1** as a catalyst for the hydrosilylation of CO_2. A preliminary study of the catalytic activity of **1** was performed in different deuterated solvents. Acetonitrile-d_3 was found to be the most suitable solvent for the hidrosilylation of CO_2 using catalyst **1**, this addressing solubility of the catalyst and inhibition of competitive reactions. Conversely, benzene-d_6 and chlorinated solvents such as dichlorometane-d_2 and chloroform-d_1 did not show to be a good option for different reasons. In the case of benzene-d_6, the poor solubility of the catalyst precursor prevented its use, while chlorinated solvents yielded mixtures of reaction products, including $ClSiEt_3$, as confirmed by NMR studies. Next, a temperature screening was performed for experiments containing **1** (5 mol% with respect to the hydrosilane) in acetonitrile-d_3, along with $HSiEt_3$, CO_2 (3 bar) and hexamethylbenzene as internal standard. The reactions were monitored by ^{1}H NMR at 298 K and 348 K, showing the best catalytic performance in acetonitrile-d_3 at 348 K. ^{1}H NMR measurements revealed the formation of the respective silylformate, $HC(O)OSiEt_3$ (**2a**), reaching almost full $HSiEt_3$ conversion (95 %) within 7.5 h at 348 K. This result was evidenced by a resonance observed at δ 8.12 ppm at the time that the signal at δ 3.63 ppm corresponding to the Si–H proton of the hydrosilane disappears in the ^{1}H NMR spectrum. Moreover, the influence of the catalyst loading on the activity of this catalytic system was also investigated. These studies revealed that when using catalyst loadings of 1.0 and 2.0 mol% under the same conditions, full $HSiEt_3$ conversion required 72 h and 16 h, respectively.

The success of this reaction prompted us to explore its generality. Thus, the influence of the hydrosilane nature on the activity of **1** as CO_2 hydrosilylation catalyst was studied. The **1**-catalyzed (1.0 mol%) reactions of CO_2 (3 bar) with $HSiEt_3$, $HSiMe_2Ph$, $HSiMePh_2$ and $HSiMe(OSiMe_3)_2$ in acetonitrile-d_3 at 348 K with hexamethylbenzene as internal standard were monitored by ^{1}H NMR spectroscopy (Scheme 2). The results of these experiments are summarized in Table 1 and the reaction profiles shown in Figure 1. A first view of the figure shows a significant influence of the hydrosilane nature on the catalytic activity. Using $HSiMe_2Ph$, full conversion of the starting hydrosilane to selectively afford the corresponding silylformate, $HC(O)OSiMe_2Ph$ (**2b**), was accomplished in less than two hours. However, when $HSiMePh_2$ was used as the reducing agent, a notable activity decrease was observed, probably due to the steric hindrance around the Si–H bond. Indeed, under the same reaction conditions, more than 8 hours were required to fulfill the conversion of $HSiMePh_2$ into $HC(O)OSiMePh_2$ (**2c**). In contrast, $HSiEt_3$ was comparatively much less reactive reaching a 24% conversion in 10 h. The **1**-catalyzed reactions of CO_2 with $HSiMe_2Ph$ and $HSiMePh_2$ were highly selective to the formation of the corresponding silylformate. Conversely, in the case of $HSiEt_3$ both parameters activity and selectivity decreased, and the resulting **2a** (88%) was always accompanied by CH_3OSiEt_3 and $O(SiEt_3)_2$, which were identified by ^{1}H and ^{29}Si{^{1}H} NMR spectroscopy. On the other hand, when $HSiMe(OSiMe_3)_2$ was used as reductant, no reaction was observed during the first 24 hours, and only 12% of the corresponding silylformate $HC(O)OSiMe(OSiMe_3)_2$ (**2d**) was produced after 40 hours.

Table 1. [Cp*IrCl{(MeIm)$_2$CHCOO}] (**1**) catalyzed hydrosilylation of CO_2 with different hydrosilanes.[a]

Entry	**1** (mol%)[b]	Hydrosilane	Time (h)	Conversion[c] (%)	Silylformate[c] (%)
1	5	$HSiEt_3$	7.5	95	96
2	1	$HSiEt_3$	10	24	88
3	1	$HSiMe_2Ph$	2	95	100
4	1	$HSiMePh_2$	8	95	100
5	1	$HSiMe(OSiMe_3)_2$	10	-	-

[a] Reaction conditions: hydrosilane (0.153 mmol), CO_2 (3 bar), acetonitrile-d_3 (0.50 mL), 348 K; [b] 1.0 mol% or 5.0 mol% with respect to the hydrosilane; [c] Determined by ^{1}H NMR integration using hexamethylbenzene as internal standard.

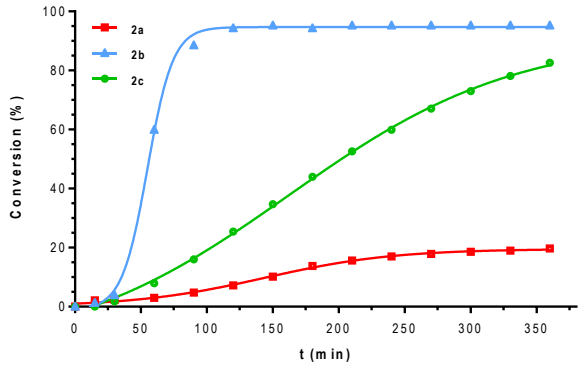

Figure 1. Hydrosilane conversion versus time for the **1**-catalyzed (1.0 mol%) reaction of CO_2 (3 bar) with $HSiEt_3$ (**2a**), $HSiMe_2Ph$ (**2b**) and $HSiMePh_2$ (**2c**) monitored by ^1H NMR in acetonitrile-d_3 at 348 K.

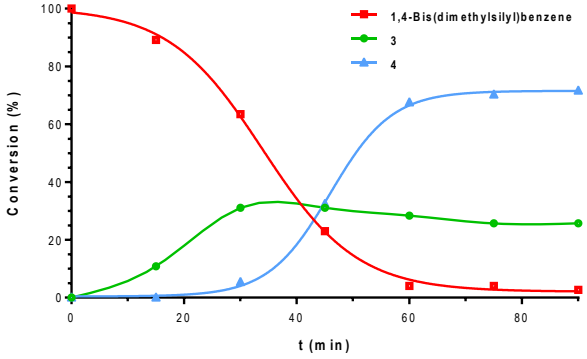

Figure 2. Time dependence of the hydrosilylation of CO_2 (3 bar) with 1,4-bis(dimethylsilyl)benzene catalyzed by **1** (1.0 mol%) monitored by ^1H NMR in acetonitrile-d_3 at 348 K.

The higher activity found for $HSiMe_2Ph$ in comparison with $HSiEt_3$ and $HSiMePh_2$, which has been attributed to a balance of steric and electronic factors, agrees with the behavior reported for Ir-NSiN[24] and Ir-NSi[12d] catalysts. However, draws attention the results obtained when using $HSiMe(OSiMe_3)_2$. The low activity found for the catalytic system **1**/$HSiMe(OSiMe_3)_2$ contrast with the activity observed for systems based on Ir-NSiN and Ir-NSi catalysts, for which the best catalytic performance was attained using HMTS. This different behavior is attributed to steric effects. Moreover, the **1**-catalyzed (1.0 mol%) reaction of 1,4-bis(dimethylsilyl)benzene with CO_2 (3 bar) in acetonitrile-d_3 at 348 K has been studied. Monitoring of the reaction by ^1H NMR evidenced the formation of 1-(dimethylsilylformate)-4-(dimethylsilyl)benzene (**3**) and 1,4-bis(dimethylsilylformate)benzene (**4**) (Scheme 3). At the early stage of the reaction, a continuous growth of the resonances corresponding to compounds **3** and **4** was observed. However, after 40 minutes the concentration of **4** increased to detriment of that of 1,4-bis(dimethylsilyl)benzene and the mono-silylformate derivative **3** (Figure 2). Notice that a 98% conversion was attained after 90 minutes to give a mixture of **4** (72%) and **3** (26%).

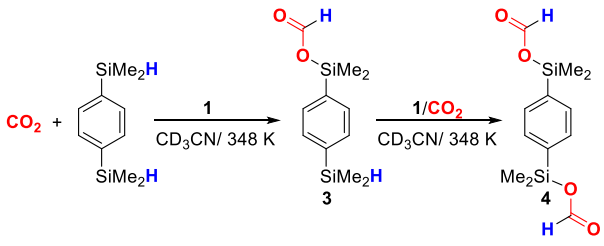

Scheme 3. Reaction of CO_2 with 1,4-bis(dimethylsilyl)benzene in acetonitrile-d_3 at 348 K catalyzed by the zwitterionic iridium species [Cp*IrCl{(MeIm)$_2$CHCOO}] (**1**) (1.0 mol%).

To ascertain the role of the uncoordinated carboxylate fragment on the catalytic activity of **1**, the performance of the related cationic carboxylate-free iridium(III) species, [Cp*IrCl{(MeIm)$_2$CH$_2$)}][PF_6] (**5**),[25] as catalyst for the hydrosilylation of CO_2 (3 bar) with $HSiMe_2Ph$ has also been investigated. This experiment evidenced that **5** also promotes the formation of silylformate **2b** but showed to be a less active catalyst precursor than **1** (Figure 3). Indeed, under the same reaction conditions but using **5** (1.0 mol%) as precatalyst only 39% of **2b** was produced after 6 hours (Figure 3). This result demonstrates that the uncoordinated carboxylate moiety at the linker of the bis-NHC ligand in **1** plays a key role on the mechanism, speeding up the CO_2 hydrosilylation process.

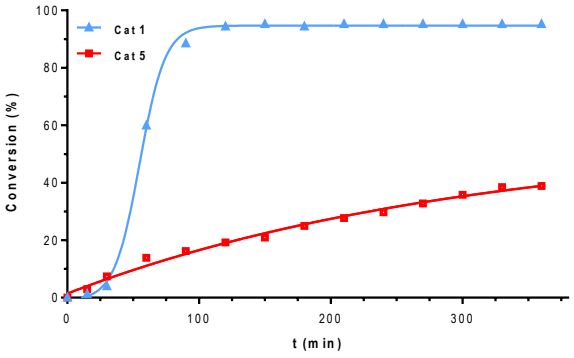

Figure 3. Hydrosilylation of CO_2 (3 bar) with $HSiMe_2Ph$ to $HC(O)OSiMe_2Ph$ (**2b**) catalyzed by [Cp*IrCl{(MeIm)$_2$CHCOO}] (**1**) and [Cp*IrCl{(MeIm)$_2$CH$_2$)}][PF_6] (**5**) (1.0 mol%) monitored by ^1H NMR in acetonitrile-d_3 at 348 K.

Theoretical calculations on the 1-catalyzed CO_2 hydrosilylation. To gain insight into the operating mechanism in the hydrosilylation of CO_2 catalyzed by **1**, a computational study using Density Functional Theory (DFT) at the B3LYP-D3BJ/def2-TZVP//def2-SVP (PCM, acetonitrile) level of theory was

performed. Within the calculations, we have considered the full structure of precatalyst **1**, as the use of model catalyst systems for this type of processes where the metallic center bears non-innocent ligands has been severely discouraged.[26] The most active reductant, $HSiMe_2Ph$, was used as a model for the hydrosilane. For the sake of clarity, the different reaction intermediates and transition structures will be referred to by capital letters, starting by precatalyst **1**, which corresponds to structure **A**. The proposed reaction mechanism is provided in Figure 4.

The theoretical calculations revealed the presence of a pre-activation step (see left part of Figure 4) that is required to form the catalytic active species (**C**). First, a ligand exchange between the chlorido ligand and a hydrosilane takes place, *via* **TSAB**. Notice that within the transition structure, the Cp* ligand changes its coordination mode from η^5 to η^1, which is possible thanks to its coordination modes flexibility.[27,28] The change in Cp* hapticity has also been proposed by other authors in similar catalytic processes.[29] This step requires to surmount an energy barrier of 25.4 kcal·mol^{-1}, which is affordable under the reaction conditions. As a result, the chlorido ligand is released, upon formation of intermediate **B**. This species is only 1.6 kcal·mol^{-1} less stable than the starting structure (**A**).

The next step involves the activation of a hydrosilane molecule by means of a ligand assisted Si–H bond cleavage.[24] This process is possible because of the high oxophilicity of silicon atoms in conjunction with the presence of an available oxygen atom in the uncoordinated carboxylate group at the bis-NHC ligand linker. For this step to proceed, an energy barrier of 18.7 kcal·mol^{-1} must be overcome, dictated by transition structure **TSBC**. Therefore, a hydride species, intermediate **C**, is produced with concomitant formation of a silyl-carboxylate moiety at the linker of the bis-NHC ligand. Notice that this step is very favorable from a thermodynamic point of view, as **C** has a relative energy of -19.3 kcal·mol^{-1}. Moreover, this step is kinetically irreversible, as the opposite process (the recovering of **B**) would require surmounting an energy barrier of 39.6 kcal·mol^{-1}, which is not at all attainable at the reaction temperature (348 K). The result of the activation step is **C**, which constitutes the active species for the subsequent catalytic cycles. On balance, the effective energy span for the catalyst activation is 25.4 kcal·mol^{-1}, according to the model proposed by Kozuch *et al.,*[30] which corresponds to the ligand exchange between the hydrosilane and the chlorido ligand.

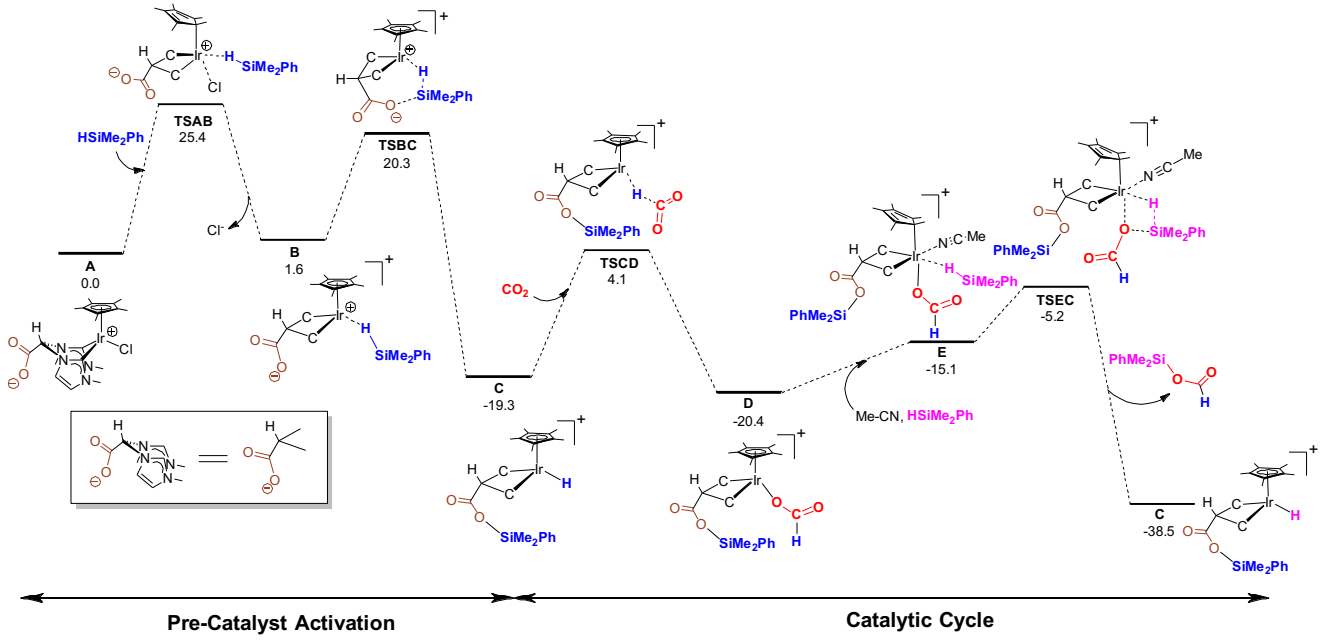

Figure 4. DFT calculated Gibbs free energy profile at 348 K (in kcal·mol^{-1}) relative to **A** and the isolated molecules.

The computed reaction profile for the catalytic cycle is presented in the right part of Figure 4. The first reaction step consists on the carbon dioxide activation by means of the hydride migration from the metallic center to the CO_2 molecule.[31] The process requires to surmount an energy barrier of 23.4 kcal·mol^{-1}, dictated by transition structure **TSCD**. As a result, the CO_2 molecule transforms into a formate ligand, which is κ^1-O-coordinated to the iridium center, yielding intermediate **D**. The silylformate product is generated by means of a σ-complex assisted metathesis (σ-CAM) between the Ir–O bond of the metallic complex and the Si–H bond of the hydrosilane, as previously proposed for other processes of hydrosilanes activation by related complexes.[32,33,34] Interestingly, within the transition state, the Cp* ligand coordinates in a η^1 manner, leaving a coordination vacancy. Consequently, the presence of a coordinating solvent, such as acetonitrile, able to stabilize the compound is essential for the reaction to proceed.

Then, upon acetonitrile coordination, intermediate **E** is produced, which can undertake the σ-CAM process via **TSEC**. Remarkably, the effective energy barrier for this process is only 15.2 kcal·mol^{-1}, being determined by the energy difference between transition structure **TSEC** and intermediate **D**. As a result, the final reaction product is yielded, and the catalytic active species **C** is regenerated. Notice that, contrarily to the previous reaction steps, this one is kinetically irreversible, as the inverse process would have to overcome an energy barrier of 33.3 kcal·mol^{-1} to take place, which is not affordable under the experimental reaction conditions (348 K).

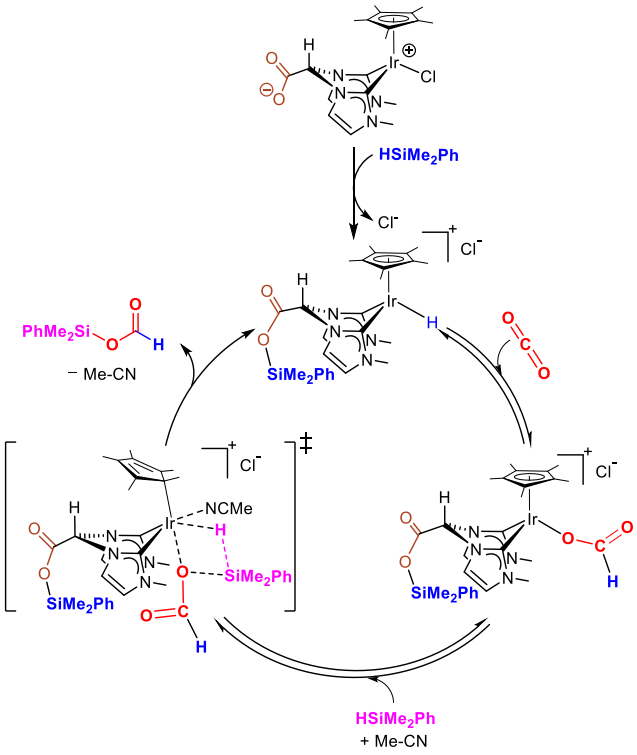

Scheme 4. Proposed mechanism for the **1**-catalyzed hydrosilylation of CO_2.

Overall, the thermodynamics for the catalytic cycle is highly favorable, with ΔG equals to -19.2 kcal·mol^{-1} (energy difference between **C** and **C** + products). The effective activation energy is 23.4 kcal·mol^{-1} and corresponds to the CO_2 fixation step. This value agrees with the experimental observations as the reaction proceeds in good yields at a temperature of 348 K. On the other hand, the effect of the solvent is crucial as contributes to the stabilization of the transition state involved in the σ-CAM process. The catalytic cycle proposed in Scheme 4 summarizes the mechanistic information obtained from experimental and theoretical studies.

^{1}H NMR studies of the reaction of **1** with 4 equiv of $HSiMe_2Ph$ at 348K in acetonitrile-d_3, in absence and in presence of CO_2 (3 bar), showed a tiny resonance at δ-16.28 ppm corresponding to traces of an Ir-hydride species which could not characterized.

1-Catalyzed reaction of secondary amines with carbon dioxide and $HSiMe_2Ph$: Synthesis of silylcarbamates. The catalytic reaction of secondary and primary amines with CO_2 using hydrosilanes as reductants has emerged as a useful methodology for the preparation of formamides, which in conjunction with proper catalysts could be further reduced to the corresponding methylamines (Scheme 5).[14,34] In view of the catalytic activity of **1** as CO_2 hydrosilylation catalyst, we decided to explore its potential as catalyst for the reductive functionalization of CO_2 with secondary amines using $HSiMe_2Ph$ as reductant.

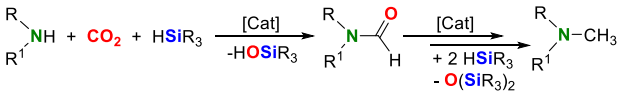

Scheme 5. Catalytic N-formylation and N-methylation of amines with CO_2 and hydrosilanes.

Preliminary studies of the **1**-catalyzed reaction of pyrrolidine, *c*-H(NC_4H_8), with CO_2 (1 bar) and one equivalent of $HSiMe_2Ph$ in acetonitrile-d_3 (0.5 mL) at 348 K showed the consumption of the starting amine to yield roughly an equimolar mixture of the corresponding silylamine, $Me_2PhSi(NC_4H_8)$ (**6a**), and silylcarbamate, $Me_2PhSiOC(O)(NC_4H_8)$ (**7a**) (Table 2, entry 1). Further addition of CO_2 (up to 3 bar) to this mixture (Figures SI61 and SI62) resulted in the full transformation of silylamine **6a** into the corresponding silylcarbamate **7a**, which was quantitatively obtained under this reaction conditions (Scheme 6). This outcome suggests that the **1**-catalyzed dehydrogenative silylation of pyrrolidine could be the driving force behind the formation of silylcarbamate **7a**.[35]

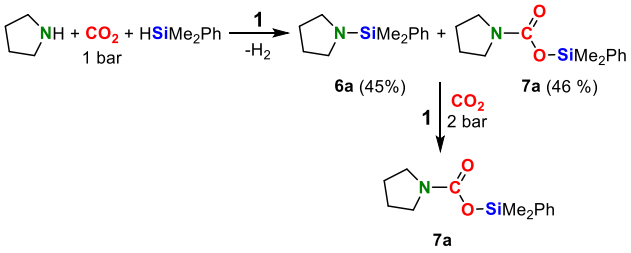

Scheme 6. Functionalization of CO_2 with pyrrolidine and $HSiMe_2Ph$ catalyzed by **1** (1.0 mol%).

Prompted by these promising results, we decided to study the **1**-catalyzed (1.0 mol%) reactions of $HSiMePh_2$ with various secondary amines, HNR_2 (NR_2 = *c*-(NC_4H_8), *c*-(NC_5H_{10}), *c*-(NC_4H_8O), NEt_2, NMe(*c*-hex) and N^{i}Pr$_2$) in acetonitrile-d_3 at 348 K. All of them, except HN^{i}Pr$_2$, were quantitatively transformed into the corresponding silylamine derivatives (Scheme 7). The reaction profiles, determined by ^{1}H NMR, displaying the hydrosilane conversion versus time are shown in Figure 5.

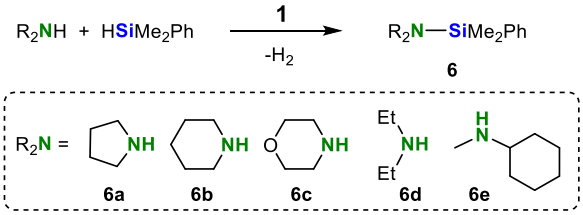

Scheme 7. Dehydrogenative silylation of amines with $HSiMe_2Ph$ catalyzed by **1** (1.0 mol%).

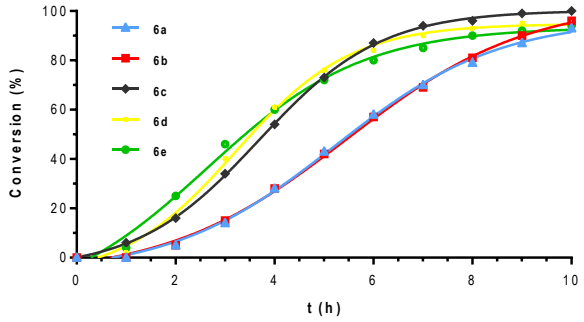

Figure 5. Hydrosilane conversion versus time for the **1**-catalyzed (1.0 mol%) reaction of $HSiMe_2Ph$ with HNR_2 (NR_2 = *c*-(NC_4H_8), *c*-(NC_5H_{10}), *c*-(NC_4H_8O), NEt_2 and NMe(*c*-hex)) monitored by ^1H NMR in acetonitrile-d_3 at 348 K.

A first view of Figure 5 shows that amines of similar nature exhibit comparable profiles. The use of secondary amines containing cyclic or acyclic aliphatic substituents such as *c*-H(NC_4H_8), *c*-H(NC_5H_{10}) *c*-H(NC_4H_8O), $HNEt_2$ and HNMe(*c*-hex), gave conversions close to 95% into the corresponding silylamines $Me_2PhSiNR_2$ (**6a-6e**) within 10 hours of reaction. However, there are some significant differences between them, the cyclic amines *c*-H(NC_4H_8) and *c*-H(NC_5H_{10}) require a preactivation step (induction time) of around 1 hour, whilst the reaction with *c*-H(NC_4H_8O) starts immediately. In this sense, a 73% conversion was attained for *c*-H(NC_4H_8O) in 5 hours whereas *c*-H(NC_4H_8) and *c*-H(NC_5H_{10}) afforded only 42% conversion at the same reaction time. $HNEt_2$, HNMe(*c*-hex) and *c*-H(NC_4H_8O) present a similar profile being the most active among the studied derivatives. No reaction was observed with bulkier amines such as HN^iPr_2 after 10 h under the same conditions. The silylamines **6a-6e** were characterized by multinuclear NMR spectroscopy (see Experimental Section and Supporting Information).

In agreement with our previous observations, the addition of CO_2 (3 bar) to the solutions containing the freshly prepared silylamines $Me_2PhSiNR_2$ (**6a-6e**) at 298 K allows for the quantitative formation of the corresponding silylcarbamates $Me_2PhSiOC(O)NR_2$ (**7a-7e**) (Scheme 8). These products, **7a-7e**, were fully characterized by ^1H, ^{29}Si and $^{13}C\{^1H\}$ NMR spectroscopy, presenting distinctive signals that demonstrate the formation of silylcarbamates. Specifically, ^1H NMR spectra of the species $Me_2PhSiOC(O)NR_2$ show a signal at δ 0.55 ppm for the methyl groups of the silyl moiety, which appears down-field shifted with respect to the parent silylamines (δ 0.30-0.36 ppm). Moreover, $^{13}C\{^1H\}$ NMR spectra exhibit the typical signal for the CO_2 insertion products at around δ 155 ppm. In addition, the $^{29}Si\{^1H\}$ NMR spectra has a resonance around δ 10.0-11.4 ppm also down-field shifted compared to that of the corresponding silylamines.

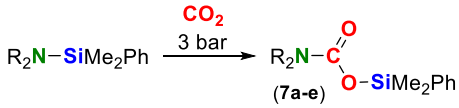

Scheme 8. Synthesis of silylcarbamates by insertion of CO_2 into the Si–N bond of silylamines.

N-formylation of amines: influence of the CO_2 pressure and amine concentration. The catalytic *N*-formylation of amines by their reaction with CO_2 and hydrosilanes is a subject of great interest.[36,39] The reaction proceeds by a series of fast and complex chemical equilibria, involving carbamate salts,[37] silylformates[38a-e] or silylcarbamates[39] as intermediates.

For the case of the **1**-catalyzed reaction of pyrrolidine with CO_2 and $HSiMe_2Ph$, it has been observed that the CO_2 pressure and amine concentration strongly influence the reaction outcome (Tables 2 and 3). To shed light on the reasons behind this behavior a series of NMR experiments were carried out.

As we have just commented, ^1H NMR evidenced that under low CO_2 pressure (1 bar), silylamine, $Me_2PhSi(NC_4H_8)$ (**6a**) (45%), and silylcarbamate, $Me_2PhSiOC(O)(NC_4H_8)$ (**7a**) (46%), are obtained as products (Table 2, entry 1).

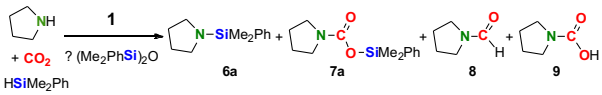

Table 2. Effect of the CO_2 pressure in the **1**-catalyzed reaction of pyrrolidine with CO_2 and $HSiMe_2Ph$.[a],[b]

Entry	CO_2 (bar)	**6a** (%)	**7a** (%)	**8** (%)	**9** (%)	f.a.[c] (%)
1	1	45	46	-	-	9
2	1.5	13	53	13	-	21
3	2	-	61	24	15	-
4	3	-	52	30	18	-

[a] Conditions: $HSiMe_2Ph$ (0.5 mmol), *c*-H(NC_4H_8) (0.5 mmol) in acetonitrile-d_3 (0.50 mL) at 348 K for 15 h. [b] 1.0 mol% of **1** with respect to the hydrosilane. (%) Determined by ^1H NMR integration using hexamethylbenzene as internal standard. [c] f.a. = free amine.

As the pressure of CO_2 is increased to 1.5 bar, a mixture of products, silylamine **6a**, silylcarbamate **7a**, formamide HC(O)(NC_4H_8) (**8**) and free amine was obtained (Figure SI63 and Table 2, entry 2). When the pressure of CO_2 was successively increased to 2 and 3 bar, silylcarbamate **7a** and formamide **8** along with carbamic acid derivative HOC(O)(NC_4H_8) (**9**), were

observed (Table 2, entries 3 and 4). The decrease in the amount of silylamine **6a** and the increase in that of silylcarbamate **7a** at 1.5 bar of CO_2 agrees with the reactivity studies of Schemes 6-8 that have shown that **7a** is formed by CO_2 insertion into **6a** (Table 2, entry 2). In this context, it is necessary to consider that an equilibrium between free amine and carbamic acid is stablished under reaction conditions (see Figures SI65, SI66).[40] Thus, formation of silylcarbamate **7a** could also result from the reaction of carbamic acid with $HSiMe_2Ph$ (*pathway a,* Scheme 9). In agreement with this possibility, it is worth mentioning that it has been proven that, as other iridium complexes,[41] **1** catalyzes the dehydrogenative silylation of formic acid with $HSiMe_2Ph$ to give the silylformate **2b** and H_2 (Figure SI64). On the other hand, the equilibrium between free amine and carbamic acid is displaced to the formation of **9** as the CO_2 pressure is increased (Figure SI65) which agrees with the presence of carbamic acid **9** in the reaction medium (Table 2, entries 3 and 4).

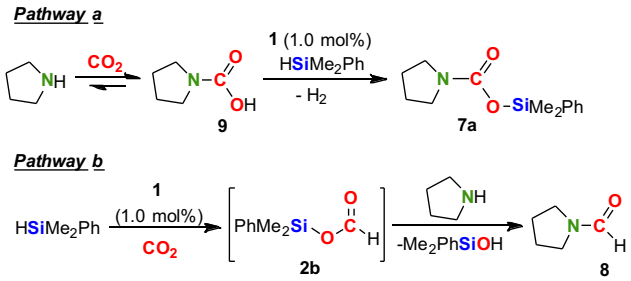

Scheme 9. Proposed mechanistic pathways for the **1**-catalyzed dehydrogenative silylation of pyrrolidine-1-carboxylic acid versus **1**-catalyzed *N*-formylation of pyrrolidine with CO_2 and $HSiMe_2Ph$.

Under 3 bar of CO_2 the selectivity in formamide product of the **1**-catalyzed reaction of pyrrolidine with the stoichiometric amount of $HSiMe_2Ph$ is surprisingly low, reaching a maximum of 30% with silylcarbamate as the major reaction product (Table 2, entry 4). In this regard, it is worth mentioning that no reaction of silylcarbamate **7a** with $HSiMe_2Ph$ has been observed at 348 K. Therefore, it is reasonable to propose that in this case formamide **8** should exclusively be generated by reaction of silylformate **2b** intermediate (not observed) with pyrrolidine (*pathway b,* Scheme 9).

To unravel the reasons behind the low selectivity in the formamide product, we have carried out a study on the influence of the relative hydrosilane and amine concentration. Experiments performed at constant CO_2 pressure (3 bar) evidenced that the reaction outcome is strongly dependent on the relative concentration of the amine and the silane (Table 3). Thus, reducing the amine and hydrosilane concentration from 0.50 mmol to 0.15 mmol resulted in the formation of formamide **8** (74%) and a 20% of the formate salt, $[H_2(NC_4H_8)][HCO_2]$ (**10**) (Table 3, entry 2).[42] The formation of **10** could only be explained by reaction of formic acid with pyrrolidine (Figure SI67). In this regard, although the presence of silanol was not detected, it is known that silanols react with silylformate in presence of amine to generate formic acid and siloxane.[36b] The decrease in the amine concentration results in a decrease in the amount of carbamic acid **9**, as a consequence of the shift of the amine/carbamic acid equilibrium, and in turn of that of the silylcarbamate **7a** (6%). This outcome supports the participation of silylformate **2b** as a reaction intermediate, which further reacts with pyrrolidine through *pathway b* (Scheme 9) to give formamide **8** and silanol. Thus, under this reaction conditions, CO_2 hydrosilylation to silylformate **2b** is favored over silylative dehydrogenation of carbamic acid to **7a**. Therefore, a significant increase on the amount of produced formamide is observed.

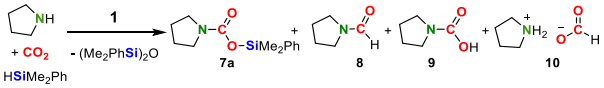

Table 3. Effect of the concentration of amine and hydrosilane in the **1**-catalyzed reaction of pyrrolidine with CO_2 and $HSiMe_2Ph$.[a],[b]
]

Entry	Amine (mmol)	$HSiMe_2Ph$ (mmol)	**7a** (%)	**8** (%)	**9** (%)	**10** (%)
1	0.50	0.50	52	30	18	-
2	0.15	0.15	6	74	-	20
3[c]	0.15	0.30	29	68	-	-
4	0.30	0.15	30	20	50	-

[a] Reaction conditions: CO_2 (3 bar), in acetonitrile-d_3 (0.50 mL) at 348 K for 15 h. [b] 1.0 mol% of **1** with respect to the reagent in lower concentration. (%) Determined by ^1H NMR integration using hexamethylbenzene as internal standard. [c] 3% of unidentified products.

Interestingly, against our initial expectations, the catalyst-free reaction of freshly prepared silylformate **2b**, which was synthesized according to a catalyst-free methodology,[43] with one equivalent of pyrrolidine quantitatively yielded a 1:1 mixture of formamide **8** and the formate salt **10** (Scheme 10). This result further supports that at least a 20% of the formamide obtained from the **1**-catalyzed reaction of pyrrolidine with CO_2 (3 bar) and $HSiMe_2Ph$ is formed via *pathway b* of Scheme 9 (Table 3, entry 2).

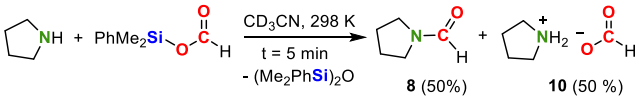

Scheme 10. Reaction of pyrrolidine with HC(O)OSiMe$_2$Ph (**2b**).

The increase of the relative hydrosilane concentration resulted in the disappearance of the formate salt **10** and an increase of that of silylcarbamate **7a** (29%) (Table 3, entry 3). This result suggests that **10** further reacts with $HSiMe_2Ph$ to give silylformate **2b** and H_2. In addition, we have found that the reaction of the formate salt **10** (independently prepared) with $HSiMe_2Ph$ in acetonitrile-d_3 at 298 K affords 1-formylpyrrolidine **8** and $O(SiMe_2Ph)_2$ with hydrogen evolution (NMR evidence, Figure SI68). On the other

hand, the shift of the amine/carbamic acid equilibrium when increasing the relative pyrrolidine concentration affords a large amount of carbamic acid **9** (50%) and silylcarbamate **7a** (30%) and, therefore, a significant decrease of formamide **8** (20%) (Table 3, entry 4). Interestingly, although the formate salt is not observed at the end of the reaction, formation of **10** has been detected by ^{1}H NMR spectroscopy along the reaction. This result indicates that under the reaction conditions *pathway b* (Scheme 9) is also an active route for the formation of **8** (Figure SI69).

The set of reactions that take place in the hydrosilylation of CO_2 with $HSiMe_2Ph$ in the presence of pyrrolidine are shown in Scheme 11. Silylformate **2b** reacts with pyrrolidine to give 1-formylpyrrolidine **8** and silanol, $HOSiMe_2Ph$. The later reacts with **2b** to afford formic acid and siloxane $O(SiMe_2Ph)_2$. In presence of pyrrolidine formic acid is neutralized to yield the pyrrolidin-1-ium formate salt **10**. Salt **10** reacts with $HSiMe_2Ph$ to produce hydrogen, **2b** and pyrrolidine. Under these conditions, **2b** and pyrrolidine reacts to produce 1-formylpyrrolidine and silanol, restarting the cycle (Scheme 11).

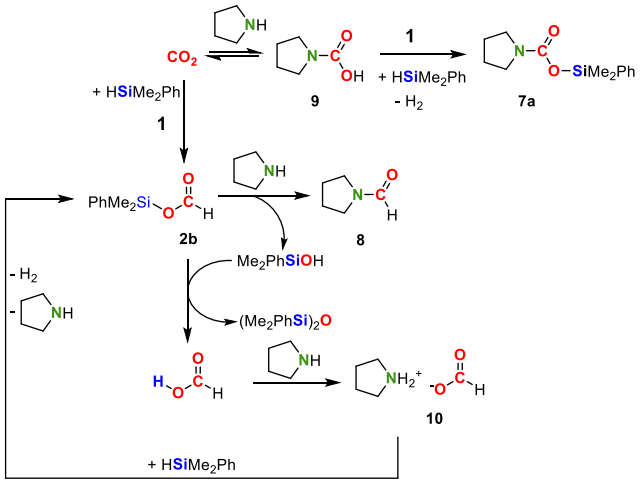

Scheme 11. Reactions involved in the **1**-catalyzed hydrosilylation of CO_2 with $HSiMe_2Ph$ in the presence of pyrrolidine

Proposed mechanistic pathways for the 1-catalyzed reactions of pyrrolidine with CO_2 and hydrosilanes.

To further understand the reaction mechanism that operates in the amine silylation process, a computational study at the same level of theory as in the formylation process was performed. We have compared the energy profile for the carboxylate silylation (catalyst **1** preactivation, steps **B** to **C** in Figure 4) with the **1**-catalyzed dehydrogenative amine silylation (**B** to **C´** in Figure 6). In particular, we have explored the direct amine silylation through a concerted process (*via* **TSBC'**), as previously proposed for similar processes.[35] As is shown in Figure 7, the amine silylation is more energetically favorable than the carboxylate silylation process with transition structure **TSBC'** being 21.6 kcal·mol^{-1} lower in energy than **TSBC**.

From **C´** there are two possible pathways: the first one consists in the CO_2 insertion into the Ir–H bond to generate a formate intermediate **D´**; which would result into the silylformate accordingly with Figure 4. This process requires to surmount an energy barrier of 24.6 kcal·mol^{-1}, dictated by **TSCD'**. The second pathway involves the elimination of the silylamine and formation of an iridium-dihydrogen intermediate **F**, the energy barrier for this step is **TSC´F** (15.9 kcal mol^{-1}). These findings allow to rationalize the reaction selectivity. At the reaction temperature (348 K) and lower CO_2 pressure, the energy barrier for the formylation process is too high to be overcome, and thus the CO_2 insertion in the silylamine, the dehydrogenative silylation product, takes place. It should be mentioned that the insertion of CO_2 into the Si–N of silylamines is a thermodynamically and kinetically favored process.[35,44] Therefore, accordingly with the experimental observations, under low CO_2 pressure silylamine and silylcarbamate should be the only expected reaction products (Table 2, entry 1). However, increasing the CO_2 pressure should favor the CO_2 activation pathway via **TSCD´** (Figure 6), enabling the formation of silylformate, which evolves according to Scheme 11. Therefore, the observed change in selectivity when increasing the CO_2 pressure (Table 2) is a consequence of the direct involvement of CO_2 in the formation of the transition state **TSCD´**. ^{1}H NMR studies of the **5**-catalyzed reaction of pyrrolidine with $HSiMe_2Ph$ under low CO_2 pressure (1 bar) showed a comparable product selectivity to that of **1**, which is agreement with the DFT calculations (Figure 6), suggesting that the carboxylate moiety at the bis-NHC ligand in **1** plays a minor role in the **1**-catalyzed reactions of pyrrolidine with CO_2 and hydrosilanes.

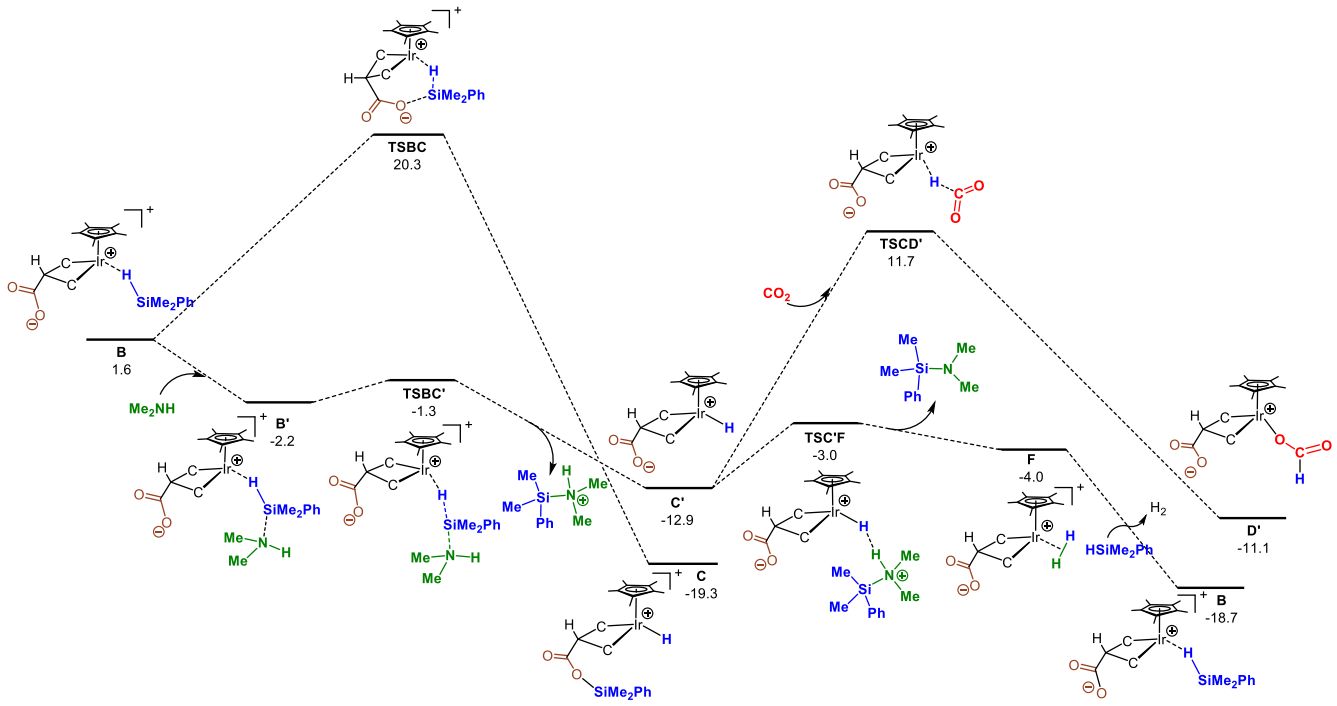

Figure 6. DFT calculated Gibbs free energy profile at 348 K (in kcal·mol^{-1}) relative to **A** and the isolated molecules for the amine silylation and posterior CO_2 activation.

Conclusions

The zwitterionic complex [Cp*IrCl{(MeIm)$_2$CHCOO}] (**1**) catalyzes the selective hydrosilylation of CO_2 with $HSiMe_2Ph$, $HSiMePh_2$, $HSiEt_3$, $HSiMe(OSiMe_3)_2$ and 1,4-bis(dimethylsilyl)benzene to the corresponding silylformate. The best reaction performance has been achieved in acetonitrile at 348 K using $HSiMe_2Ph$ as reductant. It has been proven that the carboxylate moiety at the bis-NHC ligand in **1** plays a relevant role on the catalytic mechanism. Indeed, the related carboxylate-free iridium cationic species [Cp*IrCl{(MeIm)$_2$CH$_2$)}]$^+$ (**5**) shows a poor activity as CO_2 hydrosilylation catalyst compared to **1**. In agreement with this experimental finding, theoretical calculations have revealed that the carboxylate moiety is involved in the precatalyst activation step leading to the formation of an iridium(III) hydrido active species having a silyl-carboxylate moiety at the bis-NHC linker.

Complex **1** promotes the reaction of pyrrolidine with CO_2 in the presence of $HSiMe_2Ph$ as reductant although in a non-selective way. The catalyst performance has proven to be highly dependent on both the CO_2 pressure and the relative concentration of pyrrolidine and $HSiMe_2Ph$. Thus, under a pressure of CO_2 of 3 bar and both reagents in low concentration the corresponding formamide was obtained as the major product, while at lower CO_2 pressure (1 bar) a mixture of silylamine and silylacarbamate was formed. Moreover, the **1**-catalyzed dehydrogenative silylation of *in situ* generated carbamic acid leading to silylcarbamate is also operative when increasing the pressure of CO_2. In full agreement with these observations, compound **1** efficiently catalyzes the dehydrogenative silylation of a range of secondary amines with $HSiMe_2Ph$ to afford the corresponding silylamine derivatives which further react with CO_2 (3 bar) to quantitatively afford the corresponding silylcarbamates, formed by CO_2 insertion into the Si–N bond. Theoretical calculations confirm that the dehydrogenative silylation of amines is preferred to the CO_2 hydrosilylation at low CO_2 pressure. However, increasing the CO_2 concentration favors the CO_2 hydrosilylation and therefore the formation of formamide. Interestingly, an amine-promoted pre-activation pathway leading to an iridium(III) hydrido active species, without the participation of carboxylate moiety at the bis-NHC linker, has been identified.

Reductive functionalization studies have shown that the formation of 1-formylpyrrolidine from silylformate and pyrrolidine might not be as simple as it had previously been reported. In fact, the catalyst-free reaction of silylformate with pyrrolidine in acetonitrile afforded an equimolar mixture of 1-formylpyrrolidine and the pyrrolidin-1-ium formate salt. This salt is presumably formed from the formic acid generated by reaction of the produced silanol with silylformate in presence of pyrrolidine. Interestingly, the pyrrolidin-1-ium formate salt reacts with excess of hydrosilane to give 1-formylpyrrolidine and $O(SiMe_2Ph)_2$ with hydrogen evolution.

Experimental Section

General procedures. All reactions and manipulations were performed under an argon atmosphere using Schlenk-type techniques or in a glovebox (MBraun UNIlab). Organic solvents were dried by standard procedures and distilled under an argon atmosphere prior to use or obtained oxygen- and water-free from a solvent purification system (Innovative Technologies). Acetonitrile-d_3 was dried with CaH_2 and degassed under argon prior to use. ^1H NMR, ^{13}C-APT NMR, and ^{29}Si NMR spectra were recorded on a Bruker AV-300 and AV-400 spectrometer using hexamethylbenzene as internal reference. All chemical shifts (δ) are reported in ppm and coupling constants (J) are reported in Hz and refer to apparent peak multiplicities. $^1H/^{13}C$-HSQC, $^1H/^{13}C$-HMBC and $^1H/^{29}Si$-HMBC sequences were used to assign the ^1H and $^{13}C\{^1H\}$ spectra. The iridium(III) complexes [Cp*IrCl{(MeIm)$_2$CHCOO}] (**1**)[22] and [Cp*IrCl{(MeIm)$_2$CH$_2$}][PF$_6$] (**5**)[25] were prepared following the reported procedure. Amine (pyrrolidine, pyperidine, morpholine, Et_2NH, Me(*c*-hexyl)NH and $^iPr_2NH$) and silane reagents ($HSiMe_2Ph$, $HSiMePh_2$, $HSiEt_3$ and 1,4-$(HMe_2Si)_2(C_6H_4)$) used in the catalytic experiments were purchased from commercial sources and dried over 4Å molecular sieves prior to use.

General procedure for the NMR studies of the 1-catalyzed reactions of CO_2 with $HSiR_3$. A Young NMR tube was charged with 0.153 mmol of the corresponding $HSiR_3$ (SiR_3 = $SiMe_2Ph$, $SiMePh_2$ or $SiEt_3$, complex **1** (0.89 mg, 0.00153 mmol, 1 mol%; for experiment with 5 mol %, 4.45 mg, 0.00765 mmol), CD_3CN (0.5 mL) and hexamethylbenzene (0.016 mmol, as internal standard). The tube was pressurized with CO_2 (3 bar) and the reaction was monitored by ^1H NMR at 348 K.

Data for $HC(O)OSiEt_3$ (**2a**). ^1H NMR (300 MHz, CD_3CN, 348 K): δ 8.14 (s, 1H, HC(O)O), 1.02 (t, 9H, CH_3), 0.84 (q, 6H, CH_2). ^1H NMR (300 MHz, CD_3CN, 298 K): δ 8.12 (s, 1H, HC(O)O), 0.99 (t, 3H, -CH_3), 0.80 (m, 2H, -CH_2-). ^1H-^{29}Si HMBC (80 MHz, CD_3CN, 298 K): δ 26.64 (s).

Data for $HC(O)OSiMe_2Ph$ (**2b**). ^1H NMR (300 MHz, CD_3CN, 348 K): δ 8.15 (s, 1H, HC(O)O), 7.67 (m, 2H, *o*-Ph), 7.46 (m, 3H, m, *p*-Ph), 0.60 (s, 6H, $SiMe_2$). ^1H NMR (300 MHz, CD_3CN, 298 K): δ 8.13 (s, 1H, HC(O)O), 7.67 (m, 2H, o-Ph), 7.45 (m, 3H, m, *p*-Ph), 0.58 (s, 6H, Me). ^1H-^{29}Si HMBC (80 MHz, CD_3CN, 298 K): δ 13.78 (s).

Data for $HC(O)OSiMePh_2$ (**2c**) ^1H NMR (300 MHz, CD_3CN, 348 K): δ 8.25 (s, 1H, HC(O)O), 7.68 (m, 4H, *o*-Ph), 7.46 (m, 6H, *m*, *p*-Ph), 0.90 (s, 6H, $SiMe_2$). ^1H NMR (300 MHz, CD_3CN, 298 K): δ 8.23 (s, 1H, HC(O)O), 7.66 (m, 4H, *o*-Ph), 7.45 (m, 6H, *m*, *p*-Ph), 0.89 (s, 6H, Me). $^{29}Si\{^1H\}$ NMR (80 MHz, CD_3CN, 298 K): δ 1.68 (s).

1-Catalyzed reaction of CO_2 with 1,4-bis(dimethylsilyl)benzene. A Young NMR tube was charged with 0.0765 mmol of 1,4-bis(dimethylsilyl)benzene, complex **1** (0.89 mg, 0.00153 mmol), CD_3CN (0.5 mL) and hexamethylbenzene (0.016 mmol, as internal standard). The tube was pressurized with CO_2 (3 bar) and the reaction was monitored by ^1H NMR at 348 K.

Data for {$HC(O)OSiMe_2)(C_6H_4)(SiHMe_2)$} (**3**). ^1H NMR (300 MHz, CD_3CN, 348 K): δ 8.14 (s, 1H, HC(O)O), 7.65 (d, 2H, *o*-Ph), 7.57 (d, 2H, *m*-Ph), 4.42 (m, 1H, Si-H), 0.36 (d, 6H, $SiMe_2$), 0.59 (s, 6H, $SiMe_2$). $^{29}Si\{^1H\}$ NMR plus ^1H-^{29}Si HMBC (80 MHz, CD_3CN, 298 K): δ 13.71 (s, HCO_2Si), -0.79 (s, Si-H).

Data for {$HC(O)OSiMe_2)$}$_2(C_6H_4)$ (**4**). ^1H NMR (300 MHz, CD_3CN, 348 K): δ 8.14 (s, 2H, HC(O)O), 7.72 (s, 4H, *o*-, *m*-Ph), 0.60 (s, 12H, $SiMe_2$). ^1H NMR plus HSQC (300 MHz, CD_3CN, 298 K): δ 8.12 (s, 2H, HC(O)O), 7.70 (d, 4H, *m*-, *p*-Ph), 0.58 (s, 12H, $SiMe_2$). $^{29}Si\{^1H\}$ NMR plus ^1H-^{29}Si HMBC (80 MHz, CD_3CN, 298 K): δ 13.71 (s).

General procedure for the NMR studies of the 1-catalyzed reaction of secondary amines with $HSiMe_2Ph$. A Young NMR tube was charged with 0.5 mmol of $HSiMe_2Ph$, 0.5 mmol of the corresponding secondary amine HNR_2 (NR_2 = *c*-(NC_4H_8), *c*-(NC_5H_{10}), *c*-(NC_4H_8O), NEt_2, NMe(*c*-hexyl), N^{i}Pr$_2$), complex **1** (2.9 mg, 0.005 mmol, 1 mol%), CD_3CN (0.5 mL) and hexamethylbenzene (0.016 mmol, as internal standard) and the reaction monitored by ^1H NMR at 348 K.

Data for $Me_2PhSi(NC_4H_8)$ (**6a**). ^1H NMR (300 MHz, CD_3CN, 298 K): δ 7.55 (m, 2H, *o*-Ph), 7.36 (m, 3H, *m,p*-Ph), 2.98 (t, 4H, N-CH_2-), 1.71 (q, 4H, -CH_2-), 0.33 (s, 6H, -CH_3). ^1H-^{29}Si HMBC NMR (80 MHz, CD_3CN, 298 K): δ - 4.68 (s). $^{13}C\{^1H\}$ NMR (100.6 MHz, CD_3CN, 298 K): δ 139.8 (Ph C_{ipso}), 133.6 (Ph C_o), 128.9 (Ph C_p), 127.7 (Ph C_m), 46.8 (N-CH_2-), 26.7 (-CH_2-), 3.1 (-CH_3).

Data for $Me_2PhSi(NC_5H_{10})$ (**6b**). ^1H NMR (300 MHz, CD_3CN, 298 K): δ 7.57 (m, 2H, *o*-Ph), 7.36 (m, 3H, *m,p*-Ph), 2.86 (t, 4H, N-CH_2-), 1.58 (q, 2H, -CH_2-), 1.39 (q, 4H, -CH_2-), 0.30 (s, 6H, -CH_3). ^1H-^{29}Si HMBC NMR (80 MHz, CD_3CN, 298 K): δ - 2.84 (s). $^{13}C\{^1H\}$ NMR (100.6 MHz, CD_3CN, 298 K): δ 140.0 (Ph C_{ipso}), 133.7 (Ph C_o), 128.9 (Ph C_p), 127.8 (Ph C_m), 46.5 (N-CH_2-), 27.7 (-CH_2-), 25.4 (-CH_2-), -2.7 (-CH_3).

Data for $Me_2PhSi(NC_4H_8O)$ (**6c**). ^1H NMR (300 MHz, CD_3CN, 298 K): δ 7.58 (m, 2H, *o*-Ph), 7.38 (m, 3H, *m,p*-Ph), 3.49 (t, 4H, N-CH_2-), 2.86 (t, 2H, OCH_2-), 0.33 (s, 6H, -CH_3). ^1H-^{29}Si HMBC NMR (80 MHz, CD_3CN, 298 K): δ -1.37 (s). $^{13}C\{^1H\}$ NMR (100.6 MHz, CD_3CN, 298 K): δ 140.0 (Ph C_{ipso}), 134.8 (Ph C_o), 130.1 (Ph C_p), 128.8 (Ph C_m), 69.1 (N-CH_2-), 46.6 (-OCH_2-),, -2.2 (-CH_3).

Data for $Me_2PhSiNEt_2$ (**6d**). ^1H NMR (300 MHz, CD_3CN, 298 K): δ 7.59 (m, 2H, *o*-Ph), 7.36 (m, 3H, *m,p*-Ph), 2.87 (q, 4H, -CH_2-), 1.00 (t, 6H, -CH_3), 0.33 (s, 6H, -CH_3). ^1H-^{29}Si HMBC NMR (80 MHz, CD_3CN, 298 K): δ 2.33 (s) $^{13}C\{^1H\}$ NMR (100.6 MHz, CD_3CN, 298 K): δ 141.9 (Ph C_{ipso}), 135.0 (Ph C_o), 130.0 (Ph C_p), 128.9 (Ph C_m), 41.5 (N-CH_2-), 16.6 (-CH_3), 0.73 (-CH_3).

Data for $Me_2PhSiNMe(c\text{-hex})$ (**6e**). ^1H NMR (300 MHz, CD_3CN, 298 K): δ 7.58 (m, 2H, *o*-Ph), 7.34 (m, 3H, *m,p*-Ph), 2.76 (m, 1H, N-CH-), 2.41 (s, 3H, NMe), 1.71 (m, 2H, -CH_2-), 1.57 (m, 4H, -CH_2-), 1.23 (m, 2H, -CH_2-) 1.04 (m, 2H, -CH_2-), 0.31 (s, 6H, -CH_3). ^1H-^{29}Si HMBC NMR (80 MHz, CD_3CN, 298 K): δ -2.21 (s). $^{13}C\{^1H\}$ NMR (100.6 MHz, CD_3CN, 298 K): δ 142.0 (Ph C_{ipso}), 134.9 (Ph C_o), 130.0 (Ph C_p), 128.8 (Ph C_m), 57.2 (NMe), 33.2 (-CH_2-), 29.2 (-CH-), 27.5 (-CH_2-), 27.0 (-CH_2-) , 0.9 (-CH_3).

General procedure for the NMR studies of the 1-catalyzed reaction of silylamines with CO_2 (3 bar). A Young NMR tube containing the corresponding silylamine (**6a**-**6g**; prepared from the reaction of hydrosilane Me_2PhSiH and the corresponding secondary amine HNR_2) was pressurized with CO_2 (2 or 3 bar) and the reaction monitored by ^1H NMR at 298 K.

Data for $Me_2PhSiOC(O)(NC_4H_8)$ (**7a**). ^1H NMR (300 MHz, CD_3CN, 298 K): δ 7.70 (m, 2H, *o*-Ph), 7.42 (m, 3H, *m,p*-Ph), 3.36 (m, 2H, N-CH_2-), 3.27 (m, 2H, N-CH_2-)1.83 (m, 4H, -CH_2-), 0.55 (s, 6H, -CH_3). ^1H-^{29}Si HMBC NMR (80 MHz, CD_3CN, 298 K): δ 9.74 (s). $^{13}C\{^1H\}$ NMR (100.6 MHz, CD_3CN, 298 K): δ 154.3 (-CO_2-), 137.9 (Ph C_{ipso}), 134.5 (Ph C_o), 130.9 (Ph C_p), 128.8 (Ph C_m), 47.4, 46.7 (N-CH_2-), 26.4, 25.9 (-CH_2-), -0.9 (-CH_3).

Data for $Me_2PhSiOC(O)(NC_5H_{10})$ (**7b**). ^1H NMR (300 MHz, CD_3CN, 298 K): δ 7.69 (m, 2H, *o*-Ph), 7.43 (m, 3H, *m,p*-Ph), 3.40 (m, 4H, N-CH_2-), 1.56 (m, 2H, -CH_2-), 1.51 (m, 4H, -CH_2-), 0.55 (s, 6H, -CH_3). ^1H-^{29}Si HMBC NMR

(80 MHz, CD_3CN, 298 K): δ 10.39 (s). $^{13}C\{^1H\}$ NMR (100.6 MHz, CD_3CN, 298 K): δ 154.63 (-CO_2-), 137.81 (Ph C_{ipso}), 134.5 (Ph C_o), 130.9 (Ph C_p), 128.8 (Ph C_m), 46.5, 45.1 (N-CH_2-), 26.7, 26.4 (-CH_2-), 25.0 (-CH_2-), -0.99 (-CH_3).

Data for $Me_2PhSiOC(O)(NC_4H_8O)$ (**7c**). ^1H NMR (300 MHz, CD_3CN, 298 K): δ 7.69 (m, 2H, *o*-Ph), 7.43 (m, 3H, *m,p*-Ph), 3.58 (t, 4H, O-CH_2-), 3.43 (dt, 4H, N-CH_2-), 0.56 (s, 6H, -CH_3). ^1H-^{29}Si HMBC NMR (80 MHz, CD_3CN, 298 K): δ 11.41 (s). $^{13}C\{^1H\}$ NMR (100.6 MHz, CD_3CN, 298 K): δ 154.8 (-CO_2-), 137.5 (Ph C_{ipso}), 134.5 (Ph C_o), 131.0 (Ph C_p), 129.0 (Ph C_m), 67.2 (O-CH_2-), 46.0, 44.5 (N-CH_2-), -1.1 (-CH_3).

Data for $Me_2PhSiOC(O)NEt_2$ (**7d**). ^1H NMR (300 MHz, CD_3CN, 298 K): δ 7.68 (m, 2H, *o*-Ph), 7.43 (m, 3H, *m,p*-Ph), 3.27 (m, 4H, -CH_2-), 1.12 (m, 6H, -CH_3), 0.55 (s, 6H, -CH_3). ^1H-^{29}Si HMBC NMR (80 MHz, CD_3CN, 298 K): δ 10.07 (s). $^{13}C\{^1H\}$ NMR (100.6 MHz, CD_3CN, 298 K): δ 155.2 (-CO_2-), 137.9 (Ph C_{ipso}), 134.4 (Ph C_o), 130.9 (Ph C_p), 128.8 (Ph C_m), 42.8, 42.2 (-CH_2-), 14.6, 13.8 (-CH_3), -1.0 (-CH_3).

Data for $Me_2PhSiOC(O)NMe$(*c*-hex) (**7e**). ^1H NMR (300 MHz, CD_3CN, 348 K): δ 7.70 (m, 2H, *o*-Ph), 7.45 (m, 3H, *m,p*-Ph), 3.89 (m, 1H, -CH-), 2.80 (bs, 3H, -NMe), 1.82 (m, 2H,-CH_2-), 1.66 (m, 3H, -CH_2-), 1.41 (m, 4H, -CH_2-), 1.15 (m, 1H, -CH_2-), 0.57 (s, 6H, -CH_3). ^1H-^{29}Si HMBC NMR (80 MHz, CD_3CN, 298 K): δ 10.07 (s). $^{13}C\{^1H\}$ NMR (100.6 MHz, CD_3CN, 298 K): δ 155.45 (-CO_2-), 137.9 (Ph C_{ipso}), 134.4 (Ph C_o), 130.8 (Ph C_p), 128.8 (Ph C_m), 57.0, 55.6 (NMe), 31.3, 30.7 (-CH_2-), 29.5, 28.9 (-CH-), 26.6 (-CH_2-), 26.2 (-CH_2-), -0.9 (-CH_3).

General procedure for the NMR studies of the 1-catalyzed reaction of secondary amines with CO_2 and $HSiMe_2Ph$.

Procedure a: A Young NMR tube was charged with 0.5 mmol of $HSiMe_2Ph$, 0.5 mmol of *c*-H(NC_4H_8), CO_2 (1, 2 or 3 bar), complex **1** (2.9 mg, 0.005 mmol, 1 mol%), CD_3CN (0.5 mL) and hexamethylbenzene (0.016 mmol, internal standard), and the reaction monitored by ^1H NMR at 348 K.

Data for HC(O)(NC_4H_8) (**8**). ^1H NMR (300 MHz, CD_3CN, 348 K): δ 8.19 (s, 1H, HCO), 3.46 (t, 2H, -NCH_2-), 3.32 (t, 2H, -NCH_2-), 1.86 (m, 4H, -CH_2-)

Data for HOC(O)(NC_4H_8) (**9**). ^1H NMR (300 MHz, CD_3CN, 348 K): δ 11.8 (s, 1H, COOH), 3.22 (t, 4H, -NCH_2-), 1.82 (m, 4H, -CH_2-).

Procedure b: A Young NMR tube was charged with 0.153 mmol of $HSiMe_2Ph$, 0.153 mmol of *c*-H(NC_4H_8), CO_2 (3 bar), complex **1** (0.89 mg, 0.00153 mmol, 1 mol%), CD_3CN (0.5 mL) and hexamethylbenzene (0.016 mmol, as internal standard) and the reaction monitored by ^1H NMR at 348 K.

Data for [$H_2(NC_4H_8)$][HCO_2] (**10**). ^1H NMR (300 MHz, CD_3CN, 348 K): δ 10.44 (s, 2H, H_2N^+-), 8.49 (s, 1H, $HCOO^-$), 3.15 (m, 4H, NCH_2-), 1.82 (m, 4H, -CH_2-CH_2-).

Computational Methods. DFT calculations were performed using the Gaussian09 software package, D.01revision.[45] The B3LYP exchange-correlation functional,[46] in conjunction with the D3BJ dispersion correction scheme[47] was applied in energies and gradient calculations, in conjunction with the *"ultrafine"* grid. The df2-SVP basis set was used for all the geometry optimization, and energies were further refined by means of single point calculations using the def2-TZVP basis set.[48] Solvent corrections were included in all the reported calculations through the PCM model, as implemented in the G09 suite.[49] The reported Gibbs energies were calculated at 348 K, removing the translational entropy contribution from dissolved species as indicated by Morokuma et al.[50] The nature of the stationary points has been confirmed by analytical frequency analysis, and transition states were characterized by calculation of reaction paths following the intrinsic reaction coordinate.

Acknowledgements

The authors express their appreciation for the financial support from MICINN/FEDER projects PGC2018-099383-B-100 and CTQ2016-75884-P, and the Regional Government of Aragón/FEDER 2014-2020 "*Building Europe from Aragón*" (group E42_17R). J.M. acknowledges the financial support provided by the Spanish "Ministerio de Ciencia, Innovación y Universidades" (FPU14/06003). In addition, the resources from the supercomputer "Memento", technical expertise and assistance provided by BIFIZCAM (Universidad de Zaragoza) are acknowledged.

Keywords: CO_2 • hydrosilylation • formylation • iridium • NHC

[1] (a) M. Aresta, *Carbon Dioxide as Chemical Feedstock*; 1st ed.; Wiley-VCH Verlag GmBh: Weinheim, 2010; (b) M. Aresta, A. Dibenedetto, *Dalton Trans.* **2007**, 2975–2992; (c) M. Aresta, Wiley-VCH: Weinheim, 2006, ch. 1; (d) M. Aresta, A. Dibenedetto, A. Angelini, *Chem. Rev*. **2014**, *114*, 1709–1742; (e) M. Aresta, *Coord. Chem. Rev*. **2017**, *334*, 150–183; (f) Q. Liu, L. Wu, R. Jackstell, M. Beller, *Nat. Commun*. **2015**, *6*, 5933–5948; (g) Y. Li, X. Cui, K. Dong, K. Junge, M. Beller, *ACS Catal.* **2017**, *7*, 1077–1086; (h) E. V. Kondratenko, G. Mul, J. Baltrusaitis, G. O. Larrazábal, J. Pérez-Ramírez, *Energy Environ. Sci.* **2013**, *6*, 3112–3135; (i) Z. Zhang, T. Ju, J.-H. Ye, D.-G. Yu, *Synlett* **2017**, *28*, 741–750; (j) Q.-W. Song, Z.-H. Zhou, L.-N. He, *Green Chem*. **2017**, *19*, 3707–3728; (k) M. Peters, B. Köhler, W. Kuckshinrichs, W. Leitner, P. Markewitz, T. E. Müller, *ChemSusChem* **2011**, *4*, 1216–1240; (l) I. Omae, *Coord. Chem. Rev.* **2012**, *256*, 1384–1405; (m) N. A. Tappe, R. M. Reich, V. D'Elia, F. E. Kühn, *Dalton Trans.* **2018**, *47*, 13281–13313.

[2] F. J. Fernández-Alvarez, L. A. Oro, *ChemCatChem* **2018**, *10*, 4783–4796.

[3] (a) F. J. Fernández-Alvarez, A. M. Aitani, L. A. Oro, *Catal. Sci. Technol.* **2014**, *4*, 611–624; (b) T. T. Metsänen, M. Oestreich, *Organometallics* **2015**, *34*, 543–546; (c) V. P. Taori, R. Bandari, M. R. Buchmeiser, *Chem. Eur. J.* **2014**, *20*, 3292–3296; (d) A. Berkefeld, W. E. Piers, M. Parvez, L. Castro, L. Maron, O. Eisenstein, *Chem. Sci.* **2013**, *4*, 2152–2162.

[4] For examples of Ru-based catalysts see: (a) G. Süss-Fink, J. Reiner, *J. Organomet. Chem*. **1981**, *221*, C36–C38; (b) H. Koinuma, F. Kawakami, H. Kato, H. Hirai, *J. Chem. Soc., Chem. Commun*. **1981**, 213–214; (c) P. Delgmann, E. Ember, P. Hofmann, S. Pitter, O. Walter, *Chem. Eur. J.* **2007**, *13*, 2864–2879; (d) A. Jansen, S. Pitter, *J. Mol. Catal. A: Chem.* **2004**, *217*, 41–45; (e) A. Jansen, H. Görls, S. Pitter, *Organometallics*, **2000**, *19*, 135–138.

[5] For Rh and Ir based Catalysts see: (a) R. Lalrempuia, M. Iglesias, V. Polo, P. J. Sanz Miguel, F. J. Fernández-Alvarez, J. J. Pérez-Torrente, L. A. Oro, *Angew. Chem. Int. Ed*. **2012**, *51*, 1282–12827; (b) S. Itagaki, K. Yamaguchi, N. Mizuno, *J. Mol. Catal. A: Chem.* **2013**, *366*, 347–352; (c) E. A. Jaseer, M. N. Akhtar, M. Osman, A. Al-Shammari, H. B. Oladipo, K. Garcés, F. J. Fernández-Alvarez, S. Al-Khattaf, L. A. Oro, *Catal. Sci. Technol.* **2015**, *5*, 274–279; (d) A. Julián, E. A. Jaseer, K. Garcés, F. J. Fernández-Alvarez, P. García-Orduña, F. J. Lahoz, L. A. Oro, *Catal. Sci. Technol.* **2016**, *6*, 4410–4417.

[6] For Co-based catalysts see: M. L. Scheuermann, S. P. Semproni, I. Pappas, P. J. Chirik, *Inorg. Chem*. **2014**, *53*, 9463–9465.

[7] For examples of Zn-based catalysts see: (a) W. Sattler, G. Parkin, *J. Am. Chem. Soc*. **2012**, *134*, 17462–17465; (b) W. Sattler, G. Parkin, *J. Am. Chem. Soc*. **2011**, *133*, 9708–9711.

[8] For examples of Cu-based catalysts see: (a) L. Zhang, J. Cheng, Z. Hou, *Chem. Commun*. **2013**, *49*, 4782–4784; (b) K. Motokura, D. Kashiwame, N. Takahashi, A. Miyaji, T. Baba, *Chem. Eur. J.* **2013**, *19*, 10030–10037; (c) K. Motokura, D. Kashiwame, A. Miyaji, T. Baba, *Org. Lett.* **2012**, *14*, 2642–2645.

[9] For examples of Ni-based catalysts see: (a) L. González-Sebastián, M. Flores-Alamo, J. J. García, *Organometallics* **2013**, 32, 7186–7194; (b) L. González-Sebastián, M. Flores-Alamo, J. J. García, *Organometallics* **2015**, *34*, 763–769.

[10] For examples of organocatalysts see: M.-A. Courtemanche, M.-A. Légaré, E. Rochette, F.-G. Fontaine, *Chem. Commun.* **2015**, *51*, 6858–6861.

[11] (a) Y. Jiang, O. Blacque, T. Fox, H. Berke, *J. Am. Chem. Soc.* **2013**, *135*, 7751–7760; (b) F. A. LeBlanc, W. E. Piers, M. Parvez, *Angew. Chem. Int. Ed*. **2014**, *53*, 789–792.

[12] (a) T. C. Eisenschmid, R. Eisenberg, *Organometallics* **1989**, *8*, 1822–1824; (b) S. N. Riduan, Y. Zhang, J. Y. Ying, *Angew. Chem. Int. Ed.* **2009**, *48*, 3322–3325; (c) S. N. Riduan, J. Y. Ying, Y. Zhang, *ChemCatChem* **2013**, *5*, 1490–1496; (d) J. Guzmán, P. García-Orduña, V. Polo, F. J. Lahoz, L. A. Oro, F. J. Fernández-Alvarez, *Catal. Sci. Technol*. **2019**, *9*, 2858-2867.

[13] (a) T. Matsuo, H. Kawaguchi, *J. Am. Chem. Soc.* **2006**, *128*, 12362–12363; (b) A. Berkefeld, W. E. Piers, M. Parvez, *J. Am. Chem. Soc.* **2010**, *132*, 10660–10661; (c) M. Khandelwal, R. J. Wehmschulte, *Angew. Chem. Int. Ed.* **2012**, *51*, 7323–7326; (d) S. Park, D. Bézier, M. Brookhart, *J. Am. Chem. Soc*. **2012**, *134*, 11404–11407; (e) S. J. Mitton, L. Turculet, *Chem. Eur. J.* **2012**, *18*, 15258–15262; (f) R. J. Wehmschulte, M. Saleh, D. R. Powell, *Organometallics* **2013**, *32*, 6812–6819.

[14] (a) R. A. Pramuditaa, K. Motokura, *Green Chem.* **2018**, *20*, 4834–4843; (b) J.-Y. Li, Q.-W. Song, K. Zhang, P. Liu, *Molecules* **2019**, *24*, 182–223.

[15] X. Frogneux, E. Blondiaux, P. Thuéry, T. Cantat. *ACS Catal.* **2015**, *5*, 3983–3987.

[16] D.-Y. Zhu, L. Fang, H. Han, Y. Wang, J.-B. Xia, *Org. Lett.* **2017**, *19*, 4259–4262.

[17] E. Peris, *Chem. Rev.* **2018**, *118*, 9988–10031.

[18] M. N. Hopkinson, C. Richter, M. Schedler, F. Glorius, *Nature* **2014**, *510*, 485–496.

[19] R. E. Andrew, L. González-Sebastián, A. B. Chaplin, *Dalton Trans.* **2016**, *45*, 1299–1305.

[20] (a) M. Iglesias, P. J. Sanz Miguel, V. Polo, F. J. Fernández-Alvarez, J. J. Pérez-Torrente, L. A. Oro, *Chem. Eur. J.* **2013**, *19*, 17559–17566; (b) M. Iglesias, L. A. Oro, *Chem. Soc. Rev*. **2018**, *47*, 2772–2808; (c) M. Iglesias, M. Pérez-Nicolás, P. J. Sanz Miguel, V. Polo, F. J. Fernández-Alvarez, J. J. Pérez-Torrente, L. A. Oro, *Chem Commun.* **2012**, *48*, 9480–9482.

[21] (a) R. Corberán, M.-M. Elena, E. Peris, *Eur. J. Inorg. Chem.* **2009**, *2009*, 1700–1716; (b) J. A. Mata, M. Poyatos, E. Peris, *Coord. Chem. Rev.* **2007**, *251*, 841–859.

[22] R. Puerta-Oteo, M. V. Jiménez, F. J. Lahoz, F. J. Modrego, V. Passarelli, J. J. Pérez-Torrente, *Inorg. Chem.* **2018**, *57*, 5526−5543.

[23] (a) R. Puerta-Oteo, M. Hölscher, M. V. Jiménez, W. Leitner, V. Passarelli, J. J. Pérez-Torrente, *Organometallics* **2018**, *37*, 684–696; (b) R. Puerta-Oteo, M. V. Jiménez, J. J. Pérez-Torrente, *Catal. Sci. Technol.* **2019**, *9*, 1437−1450.

[24] A. Julián, J. Guzmán, E. A. Jaseer, F. J. Fernández-Alvarez, R. Royo, P. García-Orduña, F. J. Lahoz, L. A. Oro. *Chem. Eur. J.* **2017**, *23*, 11898–11907.

[25] C. Wang, J. Liu, Z. Tian, M. Tian, L. Tian, W. Zhao, Z. Liu, *Dalton Trans*. **2017**, *46*, 6870−6883.

[26] S. A. Macgregor, *Dalton Trans.* **2011**, *40*, 11065–11065.

[27] B. F. Hallam, P. L. Pauson, *J. Chem. Soc.* **1956**, *0*, 3030–3037.

[28] C. L. Pitman, O. N. L. Finster, A. J. M. Miller, *Chem. Commun.* **2016**, *52*, 9105–9108.

[29] V. B. Kharitonov, M. Makarova, M. A. Arsenov, Y. V. Nelyubina, O. Chusova, A. S. Peregudov, S. S. Zlotskii, D. Chusov, D. A. Loginov, *Organometallics* **2018**, *37*, 2553–2562.

[30] S. Kozuch, S. Shaik, *Acc. Chem. Res.* **2011**, *44*, 101–110.

[31] A. Iturmendi, M. Iglesias, J. Munárriz, V. Polo, V. Passarelli, J. J. Pérez-Torrente, L. A. Oro. *Green Chem.* **2018**, *20*, 4875–4879.

[32] R. N. Perutz, S. Sabo-Etienne, *Angew. Chem. Int. Ed. Engl.* **2007**, *46*, 2578–2592.

[33] L. Rubio-Pérez, M. Iglesias, J. Munárriz, V. Polo, V. Passarelli, J. J. Pérez-Torrente, L. A. Oro, *Chem. Sci.* **2017**, *8*, 4811–4822.

[34] (a) X. Frogneux, E. Blondiaux, P. Thuéry, T. Cantat, *ACS Catal.* **2015**, *5*, 3983−3987; (b) A. Tlili, E. Blondiaux, X. Frogneux, T. Cantat, *Green Chem.* **2015**, *17*, 157–168; (c) I. Sorribes, K. Junge, M. Beller, *Chem. Eur. J.* **2014**, *20*, 7878–7883; (d) Y. Li, X. Fang, K. Junge, M. Beller, *Angew. Chem. Int. Ed.* **2013**, *52*, 9568–9571; (e) E. Blondiaux, J. Pouessel, T. Cantat, *Angew. Chem. Int. Ed.* **2014**, *53*, 12186–12190.

[35] A. Julián, V. Polo, E. A. Jaseer, F. J. Fernández-Alvarez, L. A. Oro, *ChemCatChem* **2015**, *7*, 3895–3902.

[36] (a) R. L. Nicholls, J. A. McManus, C. M. Rayner, J. A. Morales-Serna, A. J. P. White, B. N. Nguyen, *ACS Catal.* **2018**, *8*, 3678−3687; (b) M. Hulla, G. Laurenczy, P. J. Dyson, *ACS Catal.* **2018**, *8*, 10619−10630.

[37] (a) Z.-Z. Yang, B. Yu, H. Y. Zhang, Y. F. Zhao, G.-P. Ji, Z. M. Liu, *RSC Adv.* **2015**, *5*, 19613−19619; (b) C. Das Neves Gomes, O. Jacquet, C. Villiers, P. Thuéry, M. Ephritikhine, T. Cantat, *Angew. Chem. Int. Ed.* **2012**, *51*, 187−190.

[38] (a) T. V. Q. Nguyen, W.-J. Yoo, S. Kobayashi, *Angew. Chem. Int. Ed.* **2015**, *54*, 9209−9212; (b) S. Itagaki, K. Yamaguchi, N. Mizuno, *J. Mol. Catal. A: Chem.* **2013**, *366*, 347−352; (c) G. H. Jin, C. G. Werncke, Y. Escudié, S. Sabo-Etienne, S. Bontemps, *J. Am. Chem. Soc.* **2015**, *137*, 9563−9566; (d) L. González-Sebastián, M. Flores-Alamo, J. J. García, *Organometallics* **2013**, *32*, 7186−7194; (e) L. D. Hao, Y. F. Zhao, B. Yu, Z. Z. Yang, H. Y. Zhang, B. X. Han, X. Gao, Z. M. Liu, *ACS Catal.* **2015**, *5*, 4989−4993; (f) O. Jacquet, C. Das Neves Gomes, M. Ephritikhine, T. Cantat, *ChemCatChem* **2013**, *5*, 117−120; (g) Q. H. Zhou, Y. X. Li, *J. Am. Chem. Soc.* **2015**, *137*, 10182−10189; (h) O. Jacquet, C. Das Neves Gomes, M. Ephritikhine, T. Cantat, *J. Am. Chem. Soc.* **2012**, *134*, 2934−2937; *(i)* B. J. Wang, Z. X. Cao, *RSC Adv.* **2013**, *3*, 14007−14015.

[39] H. Lv, Q. Xing, C. Yue, Z. Lei, F. Li, *Chem. Commun.* **2016**, *52*, 6545−6548.

[40] M. Aresta, D. Ballivet-Tkatchenko, D. Belli Dell'Amico, M. C. Bonnet, D. Boschi, F. Calderazzo, R. Faure, L. Labella, F. Marchettie, *Chem. Commun.* **2000**, *1099*–1100.

[41] (a) A. Julián, K. Garcés, R. Lalrempuia, E. A. Jaseer, P. García-Orduña, F. J. Fernández-Alvarez, F. J. Lahoz, L. A. Oro, *ChemCatChem* **2018**, *10*, 1027–1034; (b) J. Guzmán, A. Torguet, P. García-Orduña, F. J. Lahoz, L. A. Oro, F. J. Fernández-Alvarez, *J. Organomet. Chem.* **2019**, *897*, 50-56.

[42] Salt **10** has been characterized by comparison of the ^{1}H and $^{13}C\{^{1}H\}$ NMR data with those obtained by us for freshly prepared **9** from the reaction of formic acid with pyrrolidine: ^{1}H NMR (300 MHz, CD_3CN, 298 K): δ 9.44 (s, 2H, H_2N^+-), 8.49 (s, 1H, HCO_2^-), 3.07 (t, 4H, -NCH_2-), 1.85 (m, 4H, -CH_2-).

[43] T. Godou, C. Chauvier, P. Thuéry, T. Cantat, *Synlett* **2017**, *28*, 2473–2477.

[44] (a) K. Kraushaar, C. Wiltzsch, J. Wagler, U. Böhme, A. Schwarzer, G. Roewer, E. Kroke, *Organometallics* **2012**, *31*, 4779−4785; (b) M. Xu, A. R. Jupp, M. S. E. Ong, K. I. Burton, S. S. Chitnis, D. W. Stephan, *Angew. Chem. Int. Ed.* **2019**, *58*, 5707–5711.

[45] M. J. Frisch, G. W. Trucks, H. B. Schlegel, G. E. Scuseria, M. A. Robb, J. R. Cheeseman, G. Scalmani, V. Barone, B. Mennucci, G. A. Petersson, H. Nakatsuji, M. Caricato, X. Li, H. P. Hratchian, A. F. Izmaylov, J. Bloino, G. Zheng, J. L. Sonnenberg, M. Hada, M. Ehara, K. Toyota, R. Fukuda, J. Hasegawa, M. Ishida, T. Nakajima, Y. Honda, O. Kitao, H. Nakai, T. Vreven, Jr. J. A. Montgomery, J. E. Peralta, F. Ogliaro, M. Bearpark, J. J. Heyd, E. Brothers, K. N. Kudin, V. N. Staroverov, R. Kobayashi, J. Normand, K. Raghavachari, A. Rendell, J. C. Burant, S. S. Iyengar, J. Tomasi, M. Cossi, N. Rega, J. M. Millam, M. Klene, J. E. Knox, J. B. Cross, V. Bakken, C. Adamo, J. Jaramillo, R. Gomperts, R. E. Stratmann,

O. Yazyev, A. J. Austin, R. Cammi, C. Pomelli, J. W. Ochterski, R. L. Martin, K. Morokuma, V. G. Zakrzewski, G. A. Voth, P. Salvador, J. J. Dannenberg, S. Dapprich, A. D. Daniels, Ö. Farkas, J. B. Foresman, J. V Ortiz, J. Cioslowski, D. J. Fox, Gaussian 09, revision D.01; Gaussian, Inc.; Wallingford CT, **2009**.

[46] A. D. Becke. *J. Chem. Phys.* **1993**, *98*, 1372–1377.

[47] (a) S. Grimme, J. Antony, S. Ehrlich, H. Krieg, *J. Chem. Phys.* **2010**, *132*, 154104. (b) E. R. Johnson, A. D. A. Becke, *J. Chem. Phys.* **2005**, *123*, 024101.

[48] F. Weigend, R. Ahlrichs, *Phys. Chem. Chem. Phys.* **2005**, *7*, 3297–3305.

[49] G. Scalmani, M. J. Frisch, *J. Chem. Phys.* **2010**, *132*, 114110.

[50] R. Tanaka, M. Yamashita, L. W. Chung, K. Morokuma, K. Nozaki, *Organometallics* **2011**, *30*, 6742–6750.

Entry for the Table of Contents (Please choose one layout)

Layout 1:

FULL PAPER

The zwitterionic iridium complex catalyzes the reduction of CO_2 with hydrosilanes to selectively afford the corresponding silylformates with the carboxylate fragment playing a key role. The mechanism of the reductive functionalization of CO_2 with amines and hydrosilanes has been investigated both experimentally and by theoretical calculations.

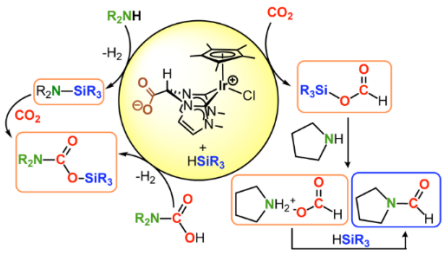

A. I. Ojeda-Amador, J. Munarriz, P. Alamán-Valtierra, V. Polo, R. Puerta-Oteo, M. V. Jiménez, F. J. Fernández-Alvarez and J. J. Pérez-Torrente**

Page No. – Page No.

Functionalization of CO_2 with Amines and Hydrosilanes Catalyzed by a Zwitterionic Iridium Carboxylate-Functionalized Bis-NHC Catalyst